On the influence of solar wind conditions on the outer-electron radiation belt

A. C. Kellerman[1,2] and Y. Y. Shprits[1,2,3]

Received 11 October 2011; revised 14 February 2012; accepted 25 March 2012; published 10 May 2012.

[1] The dependence of outer-radiation belt electron fluxes upon solar wind velocity and density is investigated using the OMNI solar wind database and LANL-GEO geosynchronous satellites for a period spanning over 20 years. Two dimensional probability distribution functions (PDF) of the flux-solar wind velocity (Vsw) and flux-solar wind density are calculated for electron energies in the 10's of keV to MeV range. The PDF's are normalized by Vsw and density and reveal new distinct relationships. Triangle-shaped flux-Vsw distributions become non-linear PDF's, and the most probable flux increases with Vsw. The only significant saturation of fluxes observed with an increase in Vsw occurs for the lower energy electron fluxes (31.7 keV). The low energy fluxes exhibit a positive correlation with solar wind density, while mid-to-high energy electron fluxes are anti-correlated with density. The maximum probability in the PDF's depends upon both velocity and density, the probability is higher for larger Vsw, and the maximum probability is larger for a given Vsw than for density. The results indicate that Vsw may be more important for determination of fluxes than density, especially for periods of high Vsw if suitable mixed delay times are applied to each solar wind parameter. It is shown that the source population of relativistic electrons of tens of keV exhibit a 2-D normalized flux-Vsw PDF, which is strikingly similar to that of the relativistic electrons. The findings support a model whereby solar wind velocity drives convective transport of source and seed electrons, to the inner magnetosphere, where local acceleration and subsequent radial diffusion is responsible for the enhanced fluxes. The results of this study also indicate that, statistically, ULF waves driven by dynamic pressure variations may act as a significant cause of loss for electrons in the 100's of keV to MeV range.

Citation: Kellerman, A. C., and Y. Y. Shprits (2012), On the influence of solar wind conditions on the outer-electron radiation belt, *J. Geophys. Res.*, *117*, A05217, doi:10.1029/2011JA017253.

1. Introduction

[2] The Earths ring current and radiation belts consist of electrons with energies of 10's of keV to several MeV. The latter are of a high enough energy to be potentially dangerous for space-borne equipment [e.g., *Baker et al.*, 1986, 1998a]. Thus, understanding the driving mechanisms, both external and internal to the magnetosphere, leading to particle acceleration, loss and inter-magnetosphere transport are vital areas of research.

[3] The observed increase in relativistic electron flux with solar wind velocity (Vsw) is one of the most well known connections between the solar wind and the magnetosphere, and was originally observed to occur 1–2 days following elevated Vsw [*Paulikas and Blake*, 1979]. Much more recently this topic was revisited using a large data set of Los Alamos National Laboratory (LANL) satellite data, combined with OMNI solar wind data [*Reeves et al.*, 2011]. In that study, a statistical analysis was conducted to re-investigate the Vsw-relativistic-electron-flux relationship for the period 1989–2009, and it was found that the Vsw-flux distribution was non-linear for both high and low energies. The relativistic particles exhibited a Vsw-dependent and linear lower flux limit, and a Vsw-independent upper flux limit, so that the flux variance was large for low Vsw and small for high Vsw. The resulting 2-D distribution of flux versus Vsw thus exhibited a "triangle" shape [*Reeves et al.*, 2011]. In addition, it was shown that fluxes tended to be higher for a given Vsw during the declining phase years, than for solar maximum, and that the triangle-shaped distribution was most clearly observed during the declining phase. The non-linear relationship between fluxes and Vsw obtained in

[1]Institute of Geophysics and Planetary Physics, University of California, Los Angeles, California, USA.
[2]Department of Earth and Space Sciences, University of California, Los Angeles, California, USA.
[3]Department of Atmospheric Sciences, University of California, Los Angeles, California, USA.

Corresponding author: A. C. Kellerman, Institute of Geophysics and Planetary Physics, University of California, 1708 Slichter Hall, 405 Hilgard Ave., Los Angeles, CA 90095, USA. (akellerman@igpp.ucla.edu)

0148-0227/12/2011JA017253

that study begs the question: what else is responsible for driving/controlling the fluxes?

[4] There has been much investigation into the response of relativistic fluxes to solar wind parameters, inter-planetary magnetic field (IMF) orientation, and geophysical parameters [e.g., *Li et al.*, 2001; *Friedel et al.*, 2002; *Li et al.*, 2005; *Lyatsky and Khazanov*, 2008a] and on the effects of different solar storms [e.g., *Borovsky and Denton*, 2006]. The IMF polarity controls the coupling efficiency between the solar wind and the magnetosphere, with B_z negative conditions resulting in a quicker acceleration of fluxes to relativistic energies than for B_z positive [*Li et al.*, 2005]. This effect was also shown and discussed in earlier studies [*Blake et al.*, 1997; *Fung and Tan*, 1998; *Obara et al.*, 2000; *Friedel et al.*, 2002]. *Lyatsky and Khazanov* [2008b] utilized data from two GOES satellites to analyze the effects of solar wind density on relativistic particle fluxes. They considered the effect on the flux for four intervals of the cubed-root of the solar wind density and a fixed Vsw bin of 400 to ~550 km s^{-1} over the years 1997–2002 and 2003–2006. They showed that an increase in density corresponded to a decrease in flux and calculated a delay dependent correlation. The cubed-root of the density was also found to anti-correlate best at a 15-hour delay, while the Vsw correlated best at a 2-day delay. The time-scale for the relativistic electron response of 1–2 days or less has been observed by numerous authors [e.g., *Baker et al.*, 1994; *Horne et al.*, 2003, 2007], and a 2-day delay was also observed to best correlate with Vsw in the recent study by *Reeves et al.* [2011, Figure 9].

[5] The delay in response of the enhancement of relativistic electron fluxes to solar wind speed driving is thought to correspond to the time it takes to accelerate some source population (at lower energy) to relativistic energies. This acceleration mechanism may occur through particle interaction with ultra-low frequency (ULF) waves, which violate the third adiabatic invariant and may result in diffusion or transport of particles from regions of high phase space density (PSD) to low PSD [e.g., *Kellogg*, 1959; *Fälthammar*, 1965; *Green and Kivelson*, 2004]. Provided that the first and second adiabatic invariants are conserved, in the case of inward diffusion, the stronger magnetic fields encountered at lower Earth orbit necessitate particle acceleration. Steady convection dominates the motion of lower energy (~10 keV) electrons [*Liu et al.*, 2003; *Jordanova and Miyoshi*, 2005; *Miyoshi et al.*, 2006; *Thorne et al.*, 2007], acting to diffuse them inwards from geosynchronous orbit. Once at 4–6 R_E they may be accelerated locally up to MeV energies, resulting in a PSD peak, from which the MeV electrons may diffuse in either radial direction [*Shprits et al.*, 2009, Figure 7].

[6] Local acceleration may occur internally to the magnetosphere through wave particle interactions at very low frequency (VLF) [e.g., *Summers et al.*, 1998; *Omura et al.*, 2007], and by fast magnetosonic waves [*Horne et al.*, 2007], see review by *Shprits et al.* [2008]. Radiation belt electrons, when interacting with whistler-mode chorus waves have an interesting dependence upon energy: There is a theoretical- and observation-based electron energy level below which energy is taken from electrons, and given to the wave, and above which energy is transferred to the electrons resulting in acceleration [*Horne et al.*, 2003]. The latter process may result in pitch angle and energy diffusion and is most effective in regions where the ratio of electron plasma frequency and gyrofrequency ω_{pe}/Ω_e is low, and for periods where a steady supply of low energy particles that excite waves, are available. The former occurs outside the plasmapause [*Tsurutani and Smith*, 1977; *Meredith et al.*, 2001, 2003], and thus during storm times, may occur as close as 4–5 R_E from Earth. The latter may occur during prolonged periods of southward B_z. Substorms, which tend to occur during periods of southward Bz, and associated strong electric fields in the nighttime magnetosphere, may also be responsible for the acceleration of lower energy particles [e.g., *Baker et al.*, 1998b]. The above mentioned phenomena may act independently or together to diffuse and accelerate particles, thus it is important to investigate the simultaneous and time-dependent variability of the low-to-high energy electron fluxes.

[7] Despite the large volume of literature on this topic, there remain many unanswered questions. For instance, in the case of solar wind driving, what is the simultaneous and/or isolated flux dependence upon Vsw, density and delay for the separate energy populations? What solar wind parameter is responsible (either directly or indirectly) for driving the flux population and under different solar cycle conditions? *Shprits et al.* [2006] showed that when the magnetopause is compressed during geomagnetic storms, fast radial diffusion acts to redistribute and smooth PSD gradients so that losses to the magnetopause are propagated down to lower L-shells, causing the flux dropouts observed at L = 4–5. It was suggested by the authors that flux dropouts would therefore be correlated with solar wind dynamic pressure (Pdyn). Thus analysis of the combined effects of Vsw and density for multiple energies should resolve any relationship with (Pdyn). The relationship between flux, density and Vsw has been investigated for extreme solar wind conditions [e.g., *Kataoka and Miyoshi*, 2008], and the Vsw and pressure effects upon fluxes have been considered during solar quiet conditions [*Takahashi and Ukhorskiy*, 2008]. A conclusion of the latter study was that the pressure may cause acceleration or loss of relativistic particles through generation of ULF waves. A recent study by *Tan et al.* [2010] showed one event where compressional-mode ULF waves may drive electron acceleration, although the long period of acceleration (~3 hours) observed in that study was not consistent with ULF waves as the only source. In addition, that study did not consider Vsw. These results clearly indicate that the driving mechanisms require further investigation. Further to this, the conflicting results add support to the notion that one must isolate the effects of each solar wind parameter if an answer to the question of the principle driving mechanism is to be found. *Lyatsky and Khazanov* [2008b] applied such a technique to investigate the effects of density and Vsw upon relativistic fluxes, for one fixed Vsw bin and for two periods containing vastly different solar wind conditions. An anti correlation between fluxes and density was observed in that study.

[8] More recently, using the *Reeves et al.* [2011] data set and an error reduction ratio method, *Balikhin et al.* [2011] established variable accounts for the most variance of relativistic fluxes at velocities >550 km s^{-1}. Specifically, they showed that the density and it's square accounted for 78% of the variance overall. In this study, we perform analysis across additional velocity and density bins and across all energies. The purpose of our analysis is to further isolate the

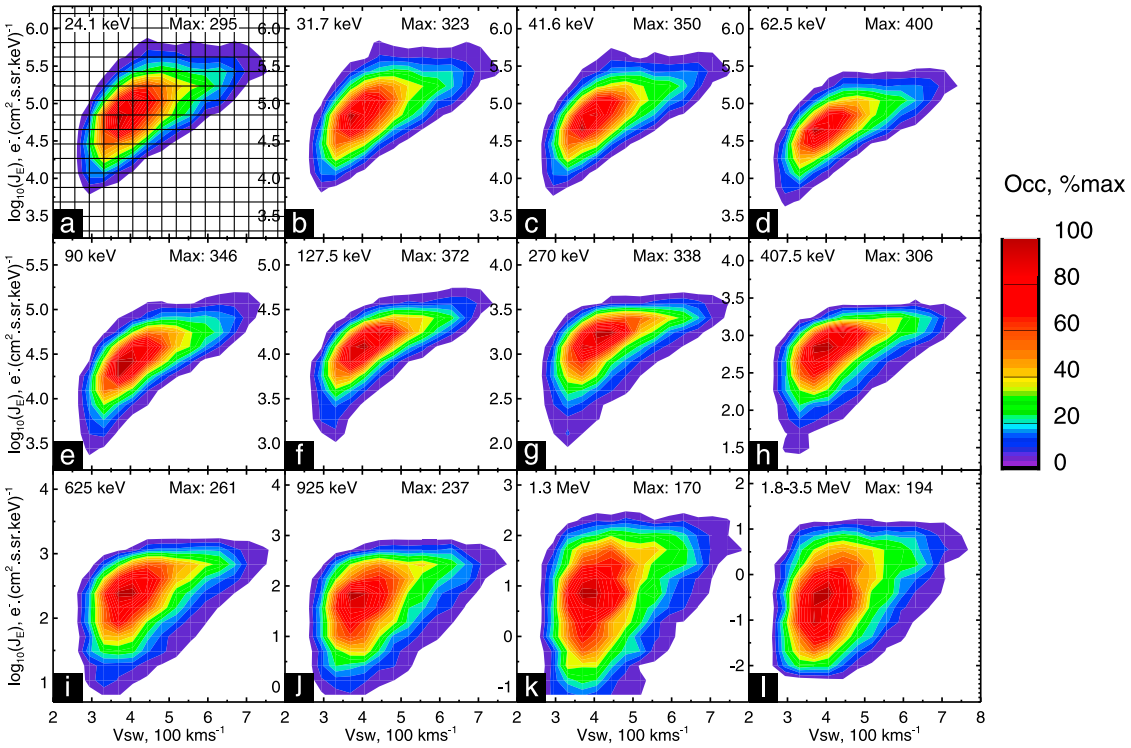

Figure 1. Two-dimensional contour plot of binned event occurrence versus the log of the electron flux (J_E) and Vsw. The data are binned into a 16 × 16 grid, as shown in Figure 1a, and then a contour calculated based on the binned points. The corresponding energy and the maximum occurrence are shown to the top left and right of each panel, respectively. The occurrence is color-coded as a percentage of the maximum in each panel, as shown to the right of the plot.

effects of one parameter over another, in order to determine the energy-dependent flux-response function to the driving mechanism under different solar conditions. A new method is introduced to conduct this analysis. We look at the probability distribution function (PDF) of the fluxes with respect to fixed velocity and density. The fluxes are shown to depend upon velocity at fixed densities, for all values of velocity and across a large range of electron fluxes for each energy, which is very instructive. We also look at the response of the relativistic fluxes, after a suitable 2-day delay is introduced to Vsw, and show that the most probable flux depends upon velocity, and that the flux probability increases for higher Vsw.

[9] The specific goals of this study are (1) to assess the effects on the flux dependence by each of Vsw and density through normalization of the solar wind distribution, (2) to re-investigate the flux dependence upon energy and solar wind conditions for fixed values of density and velocity, using probability distributions to determine the relative importance of each parameter, to (3) to determine the most probable scenario for enhancement of the outer-radiation belt electrons.

2. Instrumentation and Data Processing

[10] In this study, we utilize a long data set of daily averaged LANL satellite fluxes and OMNI solar wind data covering a period of approximately 20.25 years. The daily averaged fluxes are provided as auxiliary material in a recent publication [*Reeves et al.*, 2011], and are produced in such a way as to aid long-term studies of geosynchronous energy fluxes. All seven LANL-GEO satellites are included so as to average any effects related to a specific satellite's position and local time i.e. different L-shells, pitch angles and orbit aliasing due to field changes and satellite drift. Since the observational period of 1989-046 covers all other satellite periods, its flux measurements were used as a baseline, and all other satellite fluxes were scaled by linear regression, and averaged by weighting the error in the fit [*Reeves et al.*, 2011]; the reader is referred to the published paper and auxiliary material (ftp://ftp.agu.org/apend/ja/2010ja015735) for a detailed explanation of the data processing procedure and data format.

[11] The OMNI data spans the same period and is 1-hr averaged and corrected for gaps [*Qin et al.*, 2007]. It was obtained from the Virtual Radiation Belt Observatory (ViRBO) and is available at ftp://nssdcftp.gsfc.nasa.gov/spacecraft_data/omni/omni2.text. For the purposes of this study, the solar wind data is averaged over the same daily periods as the LANL-GEO data.

3. Observations

3.1. Occurrence Distributions

[12] In this section the 2-D distribution of occurrence between the log of the electron flux (hereinafter referred to as flux), Vsw, and solar wind ion number density (herein referred to as density) are presented and investigated.

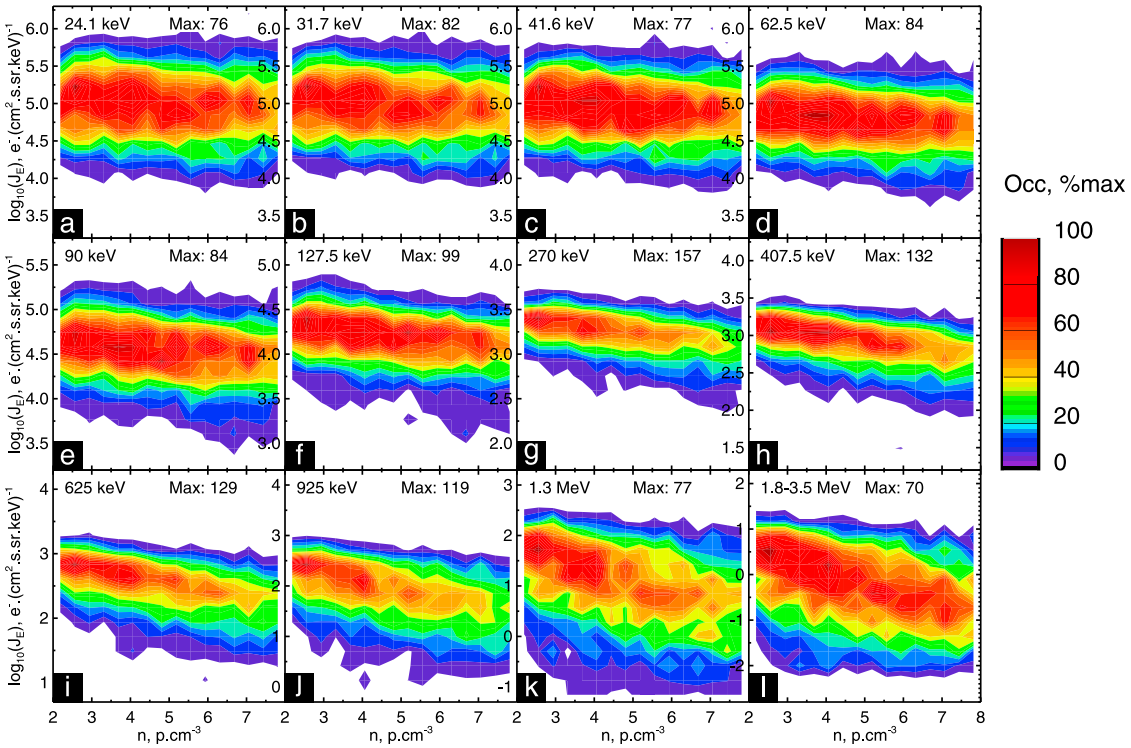

Figure 2. Similar format to Figure 1 except for density.

[13] In Figure 1 data from all available years (section 2) are organized into separate energy channels as shown to the top left of each panel. The data are then binned to a 16 × 16 grid in terms of logarithm of fluxes and solar wind speed, as displayed in panel (a). The occurrence of flux and Vsw in each 2-D bin is then determined and a contour function fitted to the gridded result. The maximum occurrence within the bins is indicated to the top right, and the contours are normalized to this maximum value. Only contours corresponding to ≥5% occurrence of max are shown. Presenting the data in this format, as opposed to scatter plots [e.g., *Reeves et al.*, 2011], clearly shows that Vsw increases with flux, however the relationship is non-linear in nature, exhibiting a roughly triangular shaped distribution, although with significant rounding of the high-flux/low-Vsw corner at low energies, and more strictly 'triangle-shaped' only at relativistic energies. For small energies the dependence of flux on Vsw is non-linear and shows evidence of saturation, however, the upper limit on the fluxes shows a strong dependence for low Vsw and an independence for high Vsw. Interestingly, the fluxes near 127.5 keV in panel (f) exhibit the smallest variance for a given value of Vsw and will be discussed later. The relativistic fluxes at 1.8–3.5 MeV in panel (l) exhibit the distinct upper-limit on flux for all values of Vsw observed by *Reeves et al.* [2011], and consistent throughout all energies is a linear lower limit as evidenced by the straight and parallel nature of the contours.

[14] Abrupt increases in high solar dynamic pressure may compress the dayside magnetopause, driving waves and causing loss of particles through outward radial diffusion to the magnetopause (section 1). The pressure depends upon Vsw, but is principally driven by density. Thus, it would be prudent to also consider the density-flux relationship. This is displayed in Figure 2 in a similar format to Figure 1, except we now plot occurrence versus flux and density. It is immediately clear that the occurrence function is significantly different here than that observed in the previous figure. There appears to be a negative correlation between the flux and density, as indicated by the decreasing slope of the contours. For low energies, the lower limit on flux shows little relationship to density increase, however as energy increases, the decrease in flux is clear for both the lower and upper limits. If we adopt the above scenario then the flux decrease, associated with higher density and pressure, may indicate a loss of relativistic particles. In addition, similar to Figure 1, there is evidence of an energy range where the fluxes exhibit a smaller variance for a given density. In this case it occurs at a higher energy near 270–407.5 keV, panels (g) and (h).

3.2. Probability Distributions

[15] In the previous section, Figure 1 illustrated the occurrence distribution of flux versus Vsw which exhibits a clear peak at Vsw ~ 350 km s^{-1}. The peak occurrence is related to the most probable Vsw. To remove this dependence of probability on the 1-D Vsw (density) distribution, in this section we calculate the 2-D probability distribution functions of the fluxes-Vsw (density) normalized by the 1-D distribution in Vsw (density), so as to find the most probable values of fluxes given a value of Vsw (density). The occurrence function itself O is related to the PDF f by $f = O/Total(O)$, where $Total(O)$ is the sum of the occurrence across all bins in O. The desired PDF thus can be calculated simply by using the occurrence. In the case of Vsw (denoted here as V) each cell in occurrence corresponds to $V \pm \Delta V$ and $J \pm \Delta J$. The 1-D Vsw occurrence distribution $O(V)$ is determined

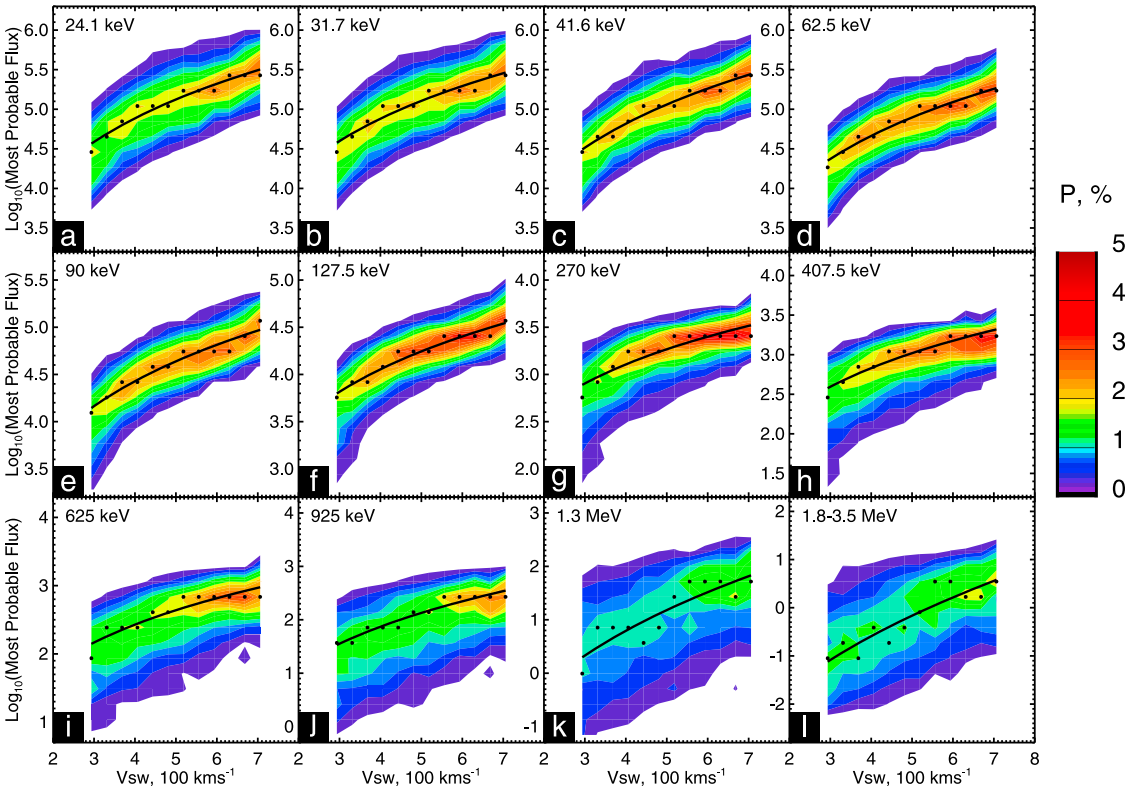

Figure 3. Two-dimensional contour plot of flux probability versus the most probable flux value and Vsw, normalized by the 1-D Vsw PDF. The flux probability (%) is shown to the right of the plot, otherwise the format is similar to Figures 1 and 2.

for the interval considered, then to obtain the normalized PDF $f'(V, J)$, we first divide each of $O(V_i \pm \Delta V, J_j \pm \Delta J)$ by $O(V_i \pm \Delta V)$ to obtain $O'(V, J)$. It should be noted that $O'(V, J)$ is a pseudo-normalized array, whereby we have that $\sum_{j=1}^{n} O'(J_j \pm \Delta J | V = V_i \pm \Delta V)$ is the same for each V_i. In order to correctly normalize the array we then divide O' by it's total, $Total(O')$, to obtain f'. Thus, for each i and j, corresponding to bins of $V \pm \Delta V$ and $J \pm \Delta J$:

$$O'(V_i \pm \Delta V, J_j \pm \Delta J) = \frac{O(\Delta V_i, J_j \pm \Delta J)}{O(V_i \pm \Delta V)}$$

$$\Rightarrow f'(V_i \pm \Delta V, J_j \pm \Delta J)_{PDF} = \frac{O'(V_i \pm \Delta V, J_j \pm \Delta J)}{Total(O')}. \quad (1)$$

[16] To explain this in terms of probability, we look at Figure 1 again. Each cell in the displayed 2-D distribution in that figure is representative of the intersection between the probability that flux lies within the interval $J_j \pm \Delta J$, and that Vsw lies within the interval $V_i \pm \Delta V$, $P(V_i \pm \Delta V \cap J_j \pm \Delta J)$. In order to remove the 1-D PDF of Vsw from the 2-D flux-Vsw PDF one must normalize it by the 1-D occurrence of Vsw i.e. Determine a conditional probability $P(J_j \pm \Delta J | V = V_i \pm \Delta V)$ for each $V_i \pm \Delta V$, so that for each $i : \sum_{j=1}^{n} P(J_j \pm \Delta J | V = V_i \pm \Delta V) = 1$, where n is the number of bins. Once the probabilities of the fluxes corresponding to each $V \pm \Delta V$ are independent, the full normalized probability function for all $V \pm \Delta V$ can be determined for each i and j by dividing by the total number of velocity bins, n: $f'(V_i \pm \Delta V, J_j \pm \Delta J)_{PDF} = \frac{1}{n} P(J_j \pm \Delta J | V_i \pm \Delta V)$, which is equal to the total (or sum) of the probabilities across all bins.

[17] Figure 3 illustrates the result of this analysis over the same period as presented in Figures 1 and 2. Cells in all the above distributions with occurrence below 5% of max are excluded to reduce errors associated with division of small numbers. The figure is color-coded in probability (%), as shown to the right, and the panels correspond to the same energies as before. Also shown is a power law fit to the maximum probability across all fluxes for each bin of $V \pm \Delta V$, the sole purpose of which is to guide the eye. The bins of maximum probability for each $V \pm \Delta V$ are shown by the black dots.

[18] The probability distributions presented in Figure 3 are significantly different from the occurrence distribution shown in Figure 1. The probability distributions provide a different insight into the flux-Vsw relationship, where we now focus on the most probable flux value for a given Vsw. The variance of the most probable flux is much smaller than the variance of the flux for a given Vsw across all energies. This shows quite clearly that maximum probability of obtaining a particular flux value depends upon Vsw, from low to high fluxes, and that the probability of obtaining the highest fluxes also depends on Vsw (as evidenced by the higher probabilities to the right of each panel). One should note though that, in this case, the probabilities below 0.25% (5% of color bar maximum) are not shown. The higher probability observed for the most

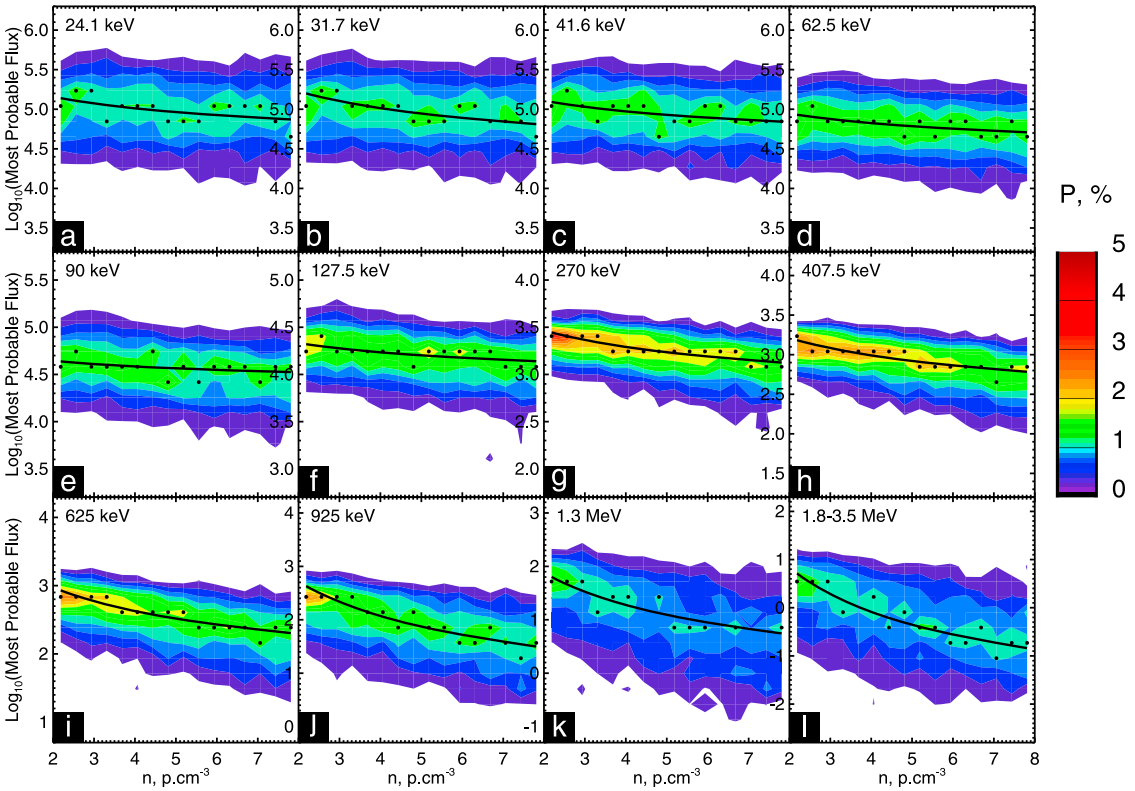

Figure 4. Similar in format to Figure 3 except that the 2-D flux-density distribution is presented and has been normalized by the 1-D density PDF.

probable flux corresponding to higher Vsw, may indicate that Vsw is more important for determining or controlling the higher flux values. The maximum probabilities for each value of Vsw are highest in panels (f)–(h), corresponding to energies of 127.5–407.5 keV, while the opposite is true for the relativistic fluxes in panels (k) and (l), where probability is very low throughout, due to a larger variance for a given Vsw.

[19] Figure 4 is produced in a similar way to Figure 3, except now density is investigated in place of Vsw. The variance of flux probability with density is significantly smaller at lower and higher energies than the flux variance for a given density value in Figure 2, and similar to the flux-density plot, an anti-correlation is observed between most probable flux and density. The probability for a given density value is quite low for the lower energies in panels (a)–(e), as compared to the dependence upon Vsw in Figure 3, and may indicate that Vsw exerts more control over the lower energy fluxes. Interestingly, the probability is distinctly highest in panels (g) and (h), corresponding to energies in the 270–407.5 keV range, which is a similar to what was observed in Figure 3. The probability of flux occurrence is also highest for lower density throughout, indicating that the highest probability of flux also depends upon density and the decrease in the most probable flux is larger for relativistic electrons than for the lower energy electrons. The above analyses, however, do not isolate the effects of velocity and density upon the most probable fluxes. The isolated effects will be investigated in the next section.

3.3. Parameter Sensitivity Analysis

[20] So far in this study the flux and most probable flux have been analyzed separately for Vsw and density, and the application of normalization to the velocity and density distributions shown in the previous section has provided further insight into the flux-Vsw and flux-density relationship. However, in order to gain an understanding of the importance of each parameter in control of the flux at various energies, one must fix one parameter while varying the other and then analyze the resultant effects. This is achieved through binning of the solar wind data. A further consideration is the previously reported delay in the relativistic electron response to Vsw (section 1). Both of these ideas are investigated in this section.

[21] The energy-dependent Vsw-flux relationship for 3 fixed bins of density is investigated in Figure 5. The density range and bin width were manually chosen so as to cover the majority of the daily averaged density distribution (Figure 2), and for illustration purposes, respectively. Each row corresponds to a density bin, as indicated at the top left of each panel and the data are normalized by the Vsw distribution corresponding to each bin, thus a different Vsw distribution is used for each row. The columns correspond to particular energies, as shown at the top left of each panel in the first row. The column furthest to the right displays the flux-Vsw distribution obtained using the value of Vsw delayed by 2 days. In each panel, a power law is fitted to the data, as explained previously, and is shown by the solid line. The bins of maximum flux probability are shown by dots again. In the bottom row, panels (k) to (o), the power-law fits from the first

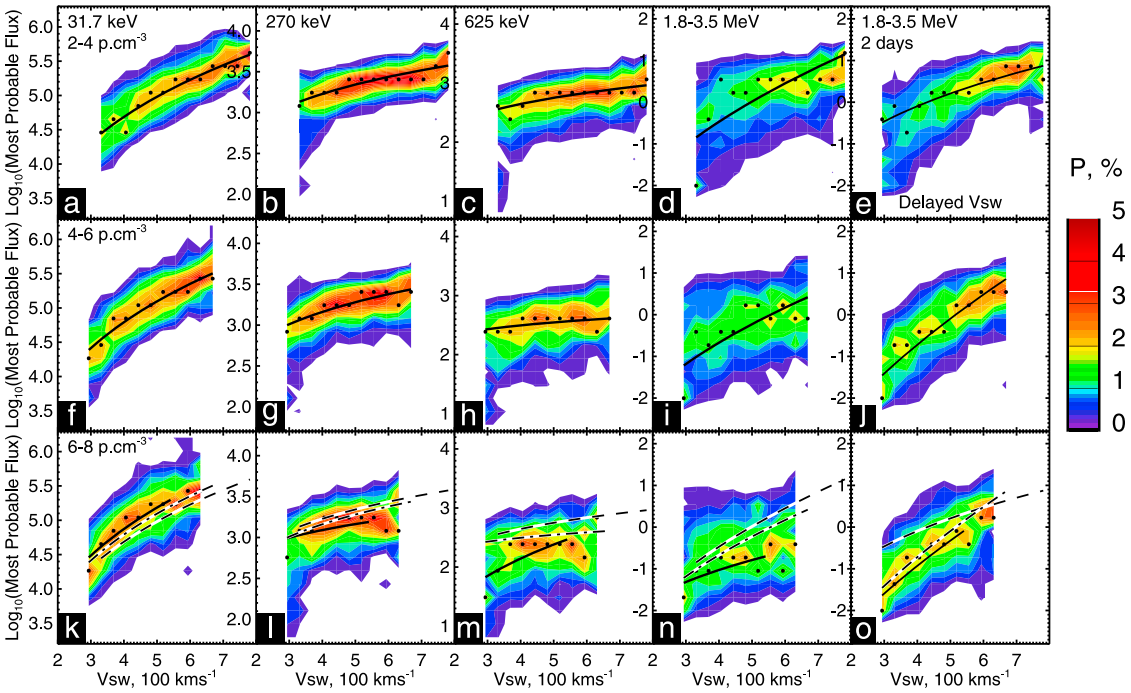

Figure 5. Two-dimensional contour plot of normalized flux probability versus most probable flux and log (Vsw) for fixed values of solar wind density. Each column corresponds to the energies considered and are shown in the top left of the panels in the first row, while each row corresponds to a fixed density, also shown at the top left of the corresponding panels. The last column to the right of the figure shows the MeV fluxes with Vsw delayed by 2 days. Polynomial fits to the maximum bins for all $Vsw \pm \Delta Vsw$ are shown in each panel by the solid line, while in the bottom row the fits from the first (second) row are shown by dashed (dot-dashed) lines.

(second) row are illustrated by dashed (dot-dashed) lines for comparison.

[22] In Figure 5a a quasi-linear response of the most probable flux-Vsw relationship is observed for low energy (31.7 keV) and density (2–4 n.cm^{-3}). This panel should be compared with Figure 3a, where a distinctly non-linear function was observed. For the 31.7 keV fluxes, an increase in the density (panels (f) and (k)) causes an increase the most probable flux level for a given Vsw, across all Vsw, as can be seen in panel (k). In addition, the flux response function becomes non-linear again, indicating that the increased density is driving the most probable fluxes to a saturation point. In panels (b) to (d) a quasi-linear increase with Vsw is observed, while increasing the density for the same energies acts to decrease the most probable fluxes (panels (l)–(n)), and change the slope. In general the flux probability is again highest for low density and high velocity.

[23] As previously mentioned, there is a delay in the response of higher-energy fluxes to Vsw. Indeed, if one investigates the response function for various delays the slope increases for the middle energies at around 1 day delay (see Figure 7). Panels (e), (j) and (o) show the relativistic flux response function for Vsw delayed by 2 days. The shape of the function is strikingly similar to the distribution functions observed for 31.7 keV, indicating that these electrons may represent the source population. The only difference observed between the two populations is in the top row, where in panel (e) a lower slope, but higher flux, is observed than for panels (j) and (o). In panel (o), it is clear that higher densities still act to reduce the fluxes.

[24] Thus far we have considered the energy-dependent effect of fixing the density and varying the Vsw on the most probable fluxes. If the delayed Vsw was considered then the density appeared to still affect the PDF of the fluxes. In Figure 6 the Vsw is restricted to 200 km s^{-1} bins and density is allowed to vary. For low energy and low Vsw a change in the density corresponds to little change in the most probable flux level, borne out by the near-horizontal slope in panel (a). This, combined with the strong relationship between the most probable flux and Vsw observed across all densities in Figure 5a would suggest near-independent control by Vsw for these energies. For higher velocities (400–600 km s^{-1}, panels (f) and (k)) the flux increases slightly with density, which is consistent with Figure 5k. The variation of the power law fits are also similar for each fixed Vsw, for 31.7 keV and 270 keV.

[25] The density at middle- to high-energies is anti-correlated with the most probable flux value, as illustrated by the negative slope. Though, in all cases except panel (k), low density and high Vsw corresponds to higher most probable fluxes, and the cases where density is high for high fixed solar wind velocity mostly have a lower flux probabilities. At 625 keV and above, the power law fits are no longer similar in variation with density. It is likely that this is due to the temporal component in the Vsw-flux relationship (~1–2 day delays for higher energies). In panels (e), (j) and (o) the Vsw is delayed by 2 days again, and an anti-correlation is evident.

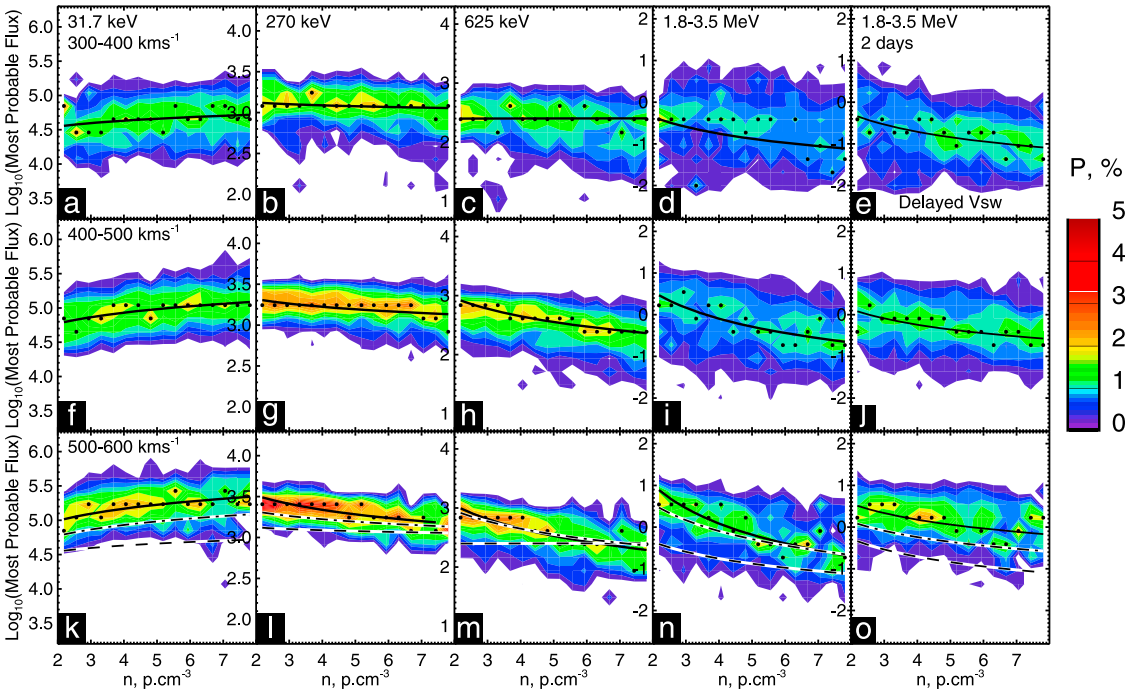

Figure 6. Similar in format to Figure 5 except for density in place of Vsw and fixed bins of Vsw are considered in place of density.

Also, the flux PDF at 37.1 keV is not representative of the flux PDF at relativistic energies. The slow decrease in relativistic flux with density for 2-day delayed Vsw shows that elevated density acts to reduce the level of the most probable relativistic fluxes over the course of a day. Further to this, the flux probability for a given density is lower than the flux probability for a given Vsw, for all electron energies, except those near 270 keV. If the lower flux probability is associated with higher variance for the given Vsw or density (i.e. control by another parameter), then this result may suggest that the velocity is more important than the density in controlling the outer radiation belt electron fluxes.

[26] A more direct way of viewing the energy-dependent relationships above is to consider only the power law fit to the most probable fluxes, all on the same axis scaling. In Figure 7 the power law curves are plotted for fixed density in the left column, and fixed velocity in the right column, and the fixed parameter bin sizes are the same as in Figures 5 and 6. The power law fits to panels (a) and (b) are shown by dotted lines in panels (e) and (f), respectively. Some additional energies have been included in this figure, and color-coded as shown to the right. Velocity is delayed by 1 minute for the calculation of the flux-Vsw PDF for 407.5 keV and 625 keV fluxes (compare 625 keV with Figures 5c, 5h and 5m), while a 2-min delayed velocity is applied to the PDF calculated for 925 keV and above. The similarity between the lower energy and higher energy curves for the fixed density cases (left column) are in support of the similar PDF's shown in Figure 5 for 31.7 keV and 1.8–3.5 MeV. In addition to this though, a steady increase in flux with Vsw is observed for low density conditions, across all energies. This supports the notion that under high velocity/low density conditions particles are accelerated from low to high energy over the course of 2 days. It should be noted though that not all features of the PDF are captured in this figure, such as the slight flattening of the curve at higher velocities, associated with saturation effects. In panel (e) higher density conditions are examined. The relativistic fluxes are lower than in panel (a), similar to what was shown previously, however, if one compares the solid and dotted curves, a relatively smooth transition to higher fluxes for higher densities is seen as the energy of the fluxes is reduced.

[27] In Figure 7, right columns, the fixed velocity cases are examined. The fitted curves look quite similar across all panels, except that the fluxes are somewhat higher for all energies when the velocity is higher, as shown previously. The effect of most probable flux increasing with density, for low energies, is also clear in this plot, as evidenced by the positive slope in the corresponding curves. The threshold energy at which the flux no longer increases with density appears to be at ~100 keV. Although there are some errors associated with the power law fits, this threshold value also appears to depend on velocity, in that more horizontal slopes are typically observed for higher energies when Vsw is lower, panel (b), as opposed to when Vsw is higher, panel (f).

3.4. Solar Cycle Dependence

[28] It has been shown thus far that the density-Vsw-flux relationship is a coupled and energy-dependent phenomenon. One further question to be addressed in this study is: If the solar wind parameters are normalized for vastly different solar wind conditions, are the relationships consistent? i.e. during solar minimum, solar maximum and during the post-maximum declining phase. To investigate this we plot the probability distribution of flux with respect to Vsw for 31.7 keV, 270 keV and 1.8–3.5 MeV (both instantaneous and Vsw delayed), and for 1997, 2000 and 2003. These years correspond to the periods mentioned above.

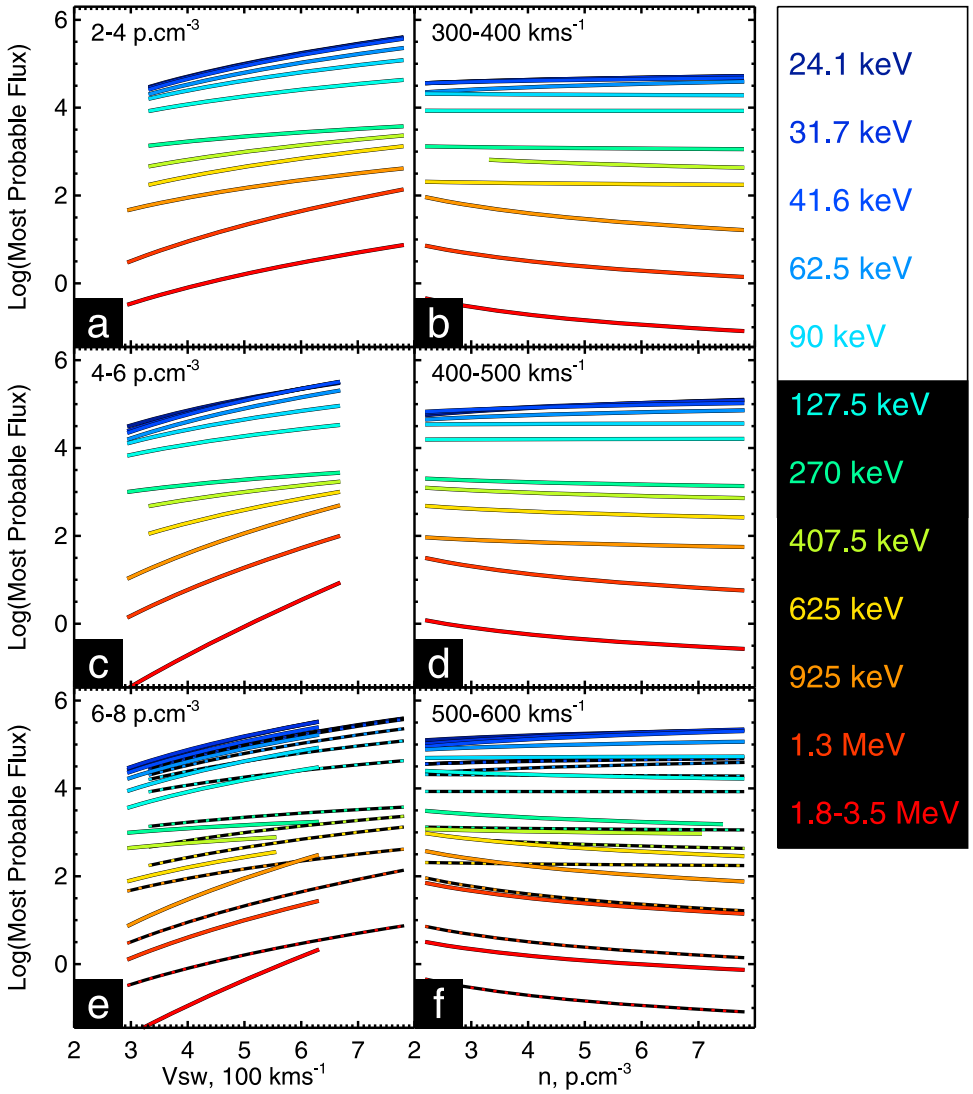

Figure 7. Summary plot of power law fits to various energies (shown to right of figure) for (left) fixed densities and (right) fixed velocities, as indicated in the top left of each panel. Here the axis scaling is the same for all energies so that the flux levels may be compared directly. Additional energies are also included, and the velocity has been delayed by 1 day for the 407.5 keV and 625 keV fluxes and for 2 days for the 925 keV and above fluxes (see text for details). The power law fitting procedure is the same as in Figures 5 and 6.

Figures 8 and 9 are displayed in a similar probability format as Figures 3 and 4, and in the right panels the fitted power-law curves are color-coded according to each year. As can be seen in panels (d) and (h) the power law fit corresponding to the maximum probability is very similar across all three years, with the agreement appearing slightly better at 31.7 keV than at 270 keV. There is evidence of a slightly higher slope for solar minimum and solar maximum years in most panels, which is consistent with higher-average density during those periods. The agreement between the flux response function to Vsw for 31.7 keV is encouraging, as it indicates that the physical mechanism behind the flux increase may be similar, if not the same across vastly different solar wind conditions, including high-solar wind stream and coronal mass ejection storms. One thing to note here is that statistics were too low to include a binned density analysis, and thus density effects are included in the response function here as they were in Figure 3.

[29] In Figures 8i–8k the instantaneous (non-delayed) most probable relativistic electron flux response is shown. The variance of the probability distribution is much higher for these energies, especially in 2000. The distribution resembles a triangle shape in 2003, and the upper most probable flux limit appears to be independent of Vsw. Further to this, the fluxes in 2003 are higher for a given Vsw than for the year 2000. Both of these results are in agreement with the scatter plots shown by *Reeves et al.* [2011], although the upper limit on most probable flux for solar maximum appears to show a dependence on Vsw, similar to Figure 3l. As has been shown in previous figures, the relativistic electron flux response for a 2-day delayed Vsw appears to be more physically significant than the

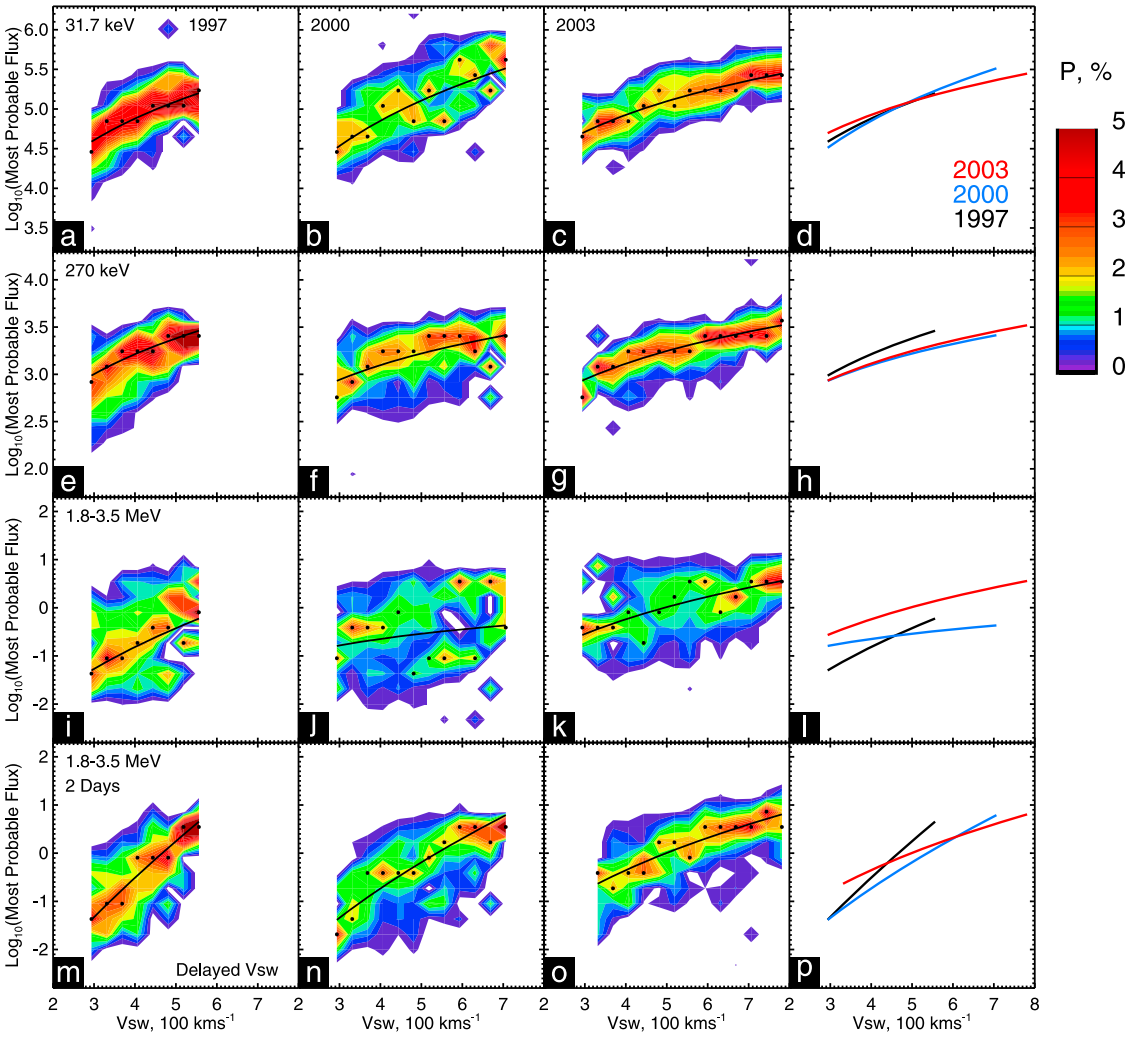

Figure 8. Two-dimensional binned and normalized flux probability versus most probable flux and log (Vsw) for three energies and for three separate years, corresponding (from left to right) to solar minimum, solar maximum and the post-maximum declining phase. Power law fits are again shown by solid lines, and maximum bins by the dots, however in the right column the lines are color-coded by year for comparison. The relativistic electron flux for 2-day delayed Vsw is also shown.

instantaneous response. This is shown in panels (m) to (o). The fits for 2000 and 2003 are very similar to the 31.7 keV response, and the upper limit on flux is similar for the available data across all years as shown in panel (p). In general the curves are rather similar across all three years, and the small variations observed may be explained by the different density and velocity conditions observed during these times; the different combinations and effects of which were summarized in Figures 5 and 6.

[30] In Figure 9 the flux-density relationship is explored in a similar format to Figure 8. The probability distribution is not well defined, in terms of a power law fit, for 31.7 keV and the 1.8–3.5 MeV energy electrons, although a general trend may still be observed. As can be seen, at 31.7 keV the slope slowly falls off with increasing density for solar minimum and solar maximum years, however it is nearly horizontal for 2003 when we expect high Vsw and low density conditions, and hence supports the notion of greater Vsw control during these times. The most probable fluxes at 31.7 keV are also highest for 2003. Interestingly, at 270 keV the flux probability is much more defined, except now the fluxes observed during 1997 and 2003 are nearly identical, and density falls off slightly more during 2000, at solar maximum. In both panels (d) and (h) the difference between the most probable fluxes during different years is greatest for larger density. In panels (i) to (k) we observe a different relationship: The most probable relativistic electron flux is highest for 2003, followed by 1997 and then solar maximum in 2000, except this time the difference in most probable flux is greatest at low density. One must bear in mind here that the effects of velocity are also included as in Figure 4, and they are not delayed. If the velocity was fixed and delayed by 2 days, we would expect to see similar relationships to those shown in Figure 6.

4. Discussion

[31] In this study a number of new techniques for analysis of the electron flux-Vsw-density relationship at

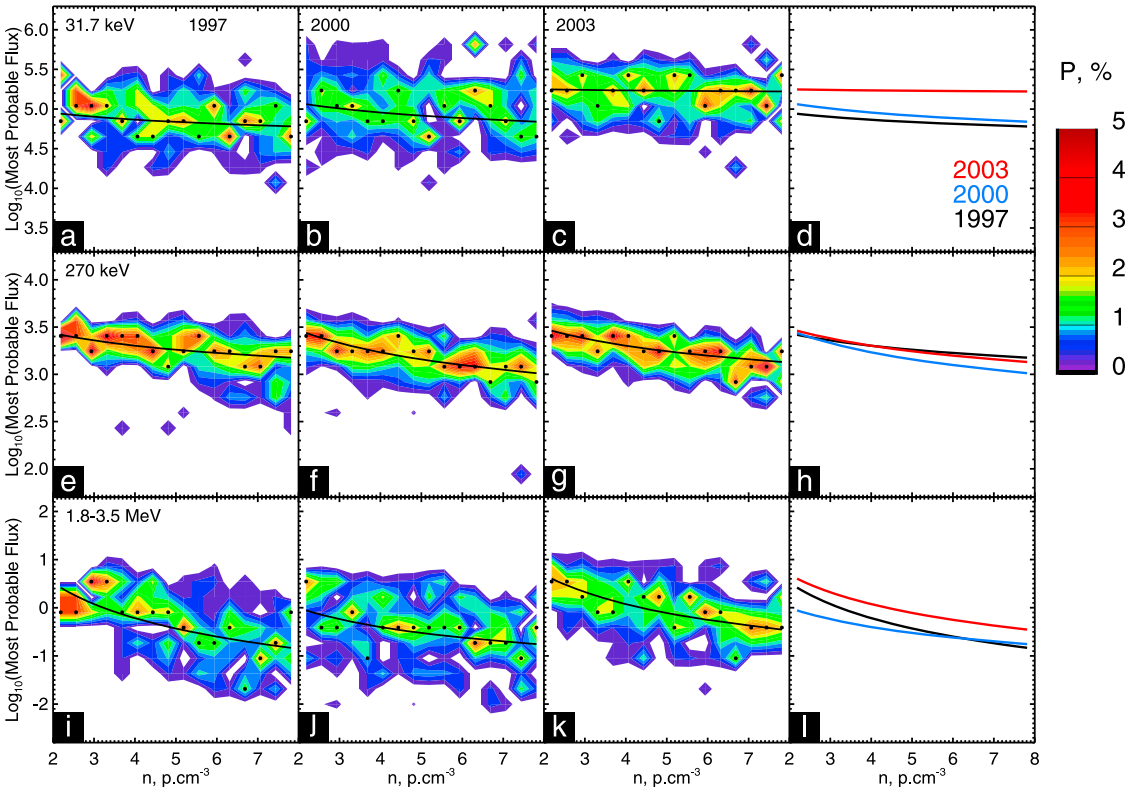

Figure 9. Similar to Figure 8 except for density in place of Vsw and excluding the 2-day delayed data.

geosynchronous orbit have been presented. Compared to previous studies, we calculated and displayed probability distribution functions in place of scatter plots and line plots. In addition, we normalized the flux PDF's by the solar wind velocity and density to remove any dependence on the 1-D PDF of the solar wind parameters. This facilitated the analysis of the flux response PDF for a given solar wind velocity or density. The simultaneous Vsw and density dependence was investigated by fixing either one parameter or the other over a number of electron energies, and the analysis has revealed a number of new results, which will be discussed in this section.

4.1. Effects of Solar Wind Density and Velocity on Geosynchronous Electron Fluxes

[32] The lower energy particles are often referred to as "source" and "seed" populations, referring to 10's and 100's of keV, respectively. Particles of these energies are a seed population for high-energy particles [e.g., *Horne et al.*, 2003], and a source population for waves [*Thorne*, 2010]. In the outer-radiation belt local acceleration of the 100's of keV energy electrons may occur through interaction with whistler mode chorus in regions of low plasma density, or by interaction with ULF waves. Periods of enhanced solar wind velocity may excite the Kelvin-Helmholtz instability on the flanks of the magnetopause, where the magnetosheath plasma flows at a speed comparable to the solar wind [e.g., *Wright et al.*, 2000], leading to the excitation of ULF waves [*Mathie and Mann*, 2001]. Solar wind dynamic pressure may also drive ULF waves and it has recently been shown that pressure may be the most important driving mechanism behind their generation [*Korotova and Sibeck*, 1995; *Kepko et al.*, 2002; *Kepko and Spence*, 2003; *Takahashi and Ukhorskiy*, 2008; *Claudepierre et al.*, 2010]. If an electrons drift period corresponds to the wavelength of the ULF wave, then a wave-particle interaction may occur, and violate the particles third adiabatic invariant, causing radial diffusion. If the diffusion occurs inwards then the particle undergoes betatron acceleration, and thus may be accelerated to relativistic energies.

[33] In this study we have considered the isolated effects of solar wind density and velocity on the most probable electron flux level, for various electron energies. The analysis of the most probable electron flux level allowed us to ascertain what flux value would most likely correspond to a given velocity or density value, and thus provides insight into the most probable conditions corresponding to acceleration and (possibly) loss of electrons. The density may be considered as a proxy for solar wind dynamic pressure. Thus, if the dynamic pressure is responsible for generation of ULF waves, and acceleration of lower energy particles, then one would expect a correlation between the relativistic electron flux and solar wind density. An anti-correlation was observed between the density and most probable flux value for mid-to-high energy electrons in Figure 6. This suggests that local acceleration by whistler-mode chorus may be primarily responsible for the acceleration of electrons observed at geosynchronous orbit.

[34] *Reeves et al.* [1998] proposed a 3-phase evolution of the radiation belt (>2 MeV) electrons during the magnetic cloud event of January 1997, using flux measurements: (1) during the acceleration phase, the electron fluxes

increased simultaneously at L ≈ 4–6; (2) as the cloud passed, the radiation belts were shifted radially outward and then relaxed earthward; and (3) after the cloud had passed the radial gradient of the fluxes flattened over a period of several days, resulting in an increase of the fluxes at higher L-shells. This scenario is in agreement with *Shprits et al.* [2009], where the source electrons (10's of keV and above) are convected inwards, accelerated locally to relativistic energies, and subsequently redistributed both inwards and outwards via radial diffusion. In this scenario an enhancement in Vsw would result in enhanced convection of electrons inwards, and thus provide additional source and seed electrons, leading to enhanced relativistic fluxes. If this scenario is indeed responsible for the enhancement then one would expect to see 1: a positive correlation between Vsw and the source and seed population electron fluxes, and 2: a similarity between the flux-Vsw PDF of two populations and that of the relativistic electron flux. Indeed, positive correlations were observed between the 31.7 keV and 270 keV electrons and Vsw in Figure 5, and a striking similarity was observed between the PDF of 31.7 keV electrons and the 2-day delayed relativistic fluxes. In addition, a smooth transition from non-delayed low energy electron fluxes to 2-day delayed relativistic fluxes was observed in Figure 7a for low density conditions. It can be surmised then, that enhanced ULF wave activity associated with periods of elevated solar wind density does not only result in radial diffusion of particles, but statistically produces significant loss of relativistic electrons. The higher flux probability for 270 keV electrons for a given density, as opposed to the 31.7 keV population, would suggest that loss of electrons through this mechanism acts also on the 'seed' electron population, ultimately contributing to a further decrease in the number of relativistic electrons. The role of electromagnetic ion cyclotron (EMIC) waves on the dynamics of the radiation belt electrons may also contribute to losses, and is currently a subject of research [*Usanova et al.*, 2008; *Ukhorskiy et al.*, 2010; *Chen et al.*, 2011].

[35] A positive correlation was observed between the source population of electrons and density. This effect was observed in Figure 5k, where the most probable 31.7 keV flux level for fixed (daily averaged) density of 6–8 p.cm^{-3} showed higher non-linearity and also reached a limit sooner than during periods of lower density, and in Figures 7b, 7d, and 7f. The positive correlation and apparent saturation of fluxes observed for this population may be explained as follows: In a recent study by *Mauk and Fox* [2010] the Kennel-Petschek limit on trapped fluxes was investigated for the five strongly magnetized planets in our solar system. They analyzed the energy dependent intensity of fluxes with respect to the Kennel-Petschek limit and showed that, for the Earth's magnetosphere, as the plasma density in the plasma sheet was increased, the low-energy fluxes approached an asymptotic limit, corresponding to the Kennel-Petschek limit. Since the plasma sheet density has been shown to correlate with solar wind density [*Borovsky et al.*, 1998], then it may be inferred that for elevated solar wind density, the lower energy population will saturate and thus exhibit a nonlinear response. The increased 31.7 keV electron flux with enhanced solar wind density shown in Figure 5k is thus consistent with transport of the solar wind particles to the magnetosphere, where they undergo convective acceleration.

[36] As previously mentioned, *Balikhin et al.* [2011, hereinafter B11] investigated the variance of the 1.8–3.5 MeV electron flux with respect to solar wind parameters, and showed that the density delayed by 1 day, and its square accounted for about 78% of the variance in the relativistic fluxes, and that 2-day delayed velocity accounted for 6%. It should be noted that inter-dependencies between parameters were considered non-existent or negligible in B11, and only simultaneous parameters were considered (i.e all parameters delayed by the same time, or not at all). In relation to the former point, a clear dependence between velocity and density exists, in that they are anti-correlated. This was evident in B11's Figure 1c, although dismissed as non-trivial in that study. In the current study, it has been shown that different results are obtained by conducting a parameter sensitivity analysis, and thus, that the Vsw-density relationship needs to be taken into account in the analysis. This may account for the discrepancy between studies promoting density as the primary driver of relativistic flux variance, to those which have promoted Vsw as the primary driver. In relation to the point made above on simultaneous parameters, B11's Figure 2 shows the relationship between instantaneous (non delayed) velocity and 1.8–3.5 MeV electron flux, for fixed densities at 1-day delay. One should compare our Figures 5d, 5i, and 5n to B11's Figures 2a–2c, although we have not delayed the density in our figure. If the Vsw is not delayed then there is an increase in the flux with velocity up to ≈550 km s^{-1}, and an apparent saturation thereafter. However, one must consider mixed delay times in order to obtain a physically correct model of the relativistic flux variances. For instance, it is well established that there is a 2-day delay between enhanced Vsw and the enhanced relativistic electron fluxes (section 1), while enhanced density, which principally drives pressure, may act to reduce fluxes over the period of a day or less [e.g., *Lyatsky and Khazanov*, 2008b]. Hence, if the velocity is delayed by 2 days and the density is not delayed (i.e. non-simultaneous parameters), then the observed "saturation" effect is significantly reduced, the triangle distribution is no longer evident, and the most probable flux exhibits a dependence upon the solar wind velocity well above 550 km s^{-1}, Figure 5e. We also showed that the probability for a given most probable flux value was higher during periods of high Vsw.

[37] The probability-based analysis used here to calculate the PDF's in Figure 5 may be applied to additional energy ranges and density bins. Fitted curves to the most probable flux, such as those shown in the figure, may then be applied to predict the relativistic fluxes at the time the solar wind information arrives at the satellite. This will form the basis of future work. Further improvements of the analysis method presented here will include the inclusion of individual satellite data on a higher time resolution, and thus for different MLT sectors. The relativistic electron flux response can also be characterized to a solar wind pressure pulse of different time duration and strength, in order to model rapid flux dropouts due to magnetopause shadowing. The combination of the above analyses will allow us to determine when and where acceleration and losses maybe taking place and on what time scale. Further to this, seasonal and IMF effects have not been considered in this study, and thus the inclusion of the associated Russell-McPherron effect may

improve the analysis, especially during equinoctial periods where fluxes may be driven to higher values.

5. Conclusions

[38] In this study a long data set of solar wind and geosynchronous electron flux data has been utilized to determine the probability based relationships between normalized solar wind density, velocity and daily averaged outer radiation belt electron fluxes. The following results were obtained:

[39] 1. Normalization of the solar wind velocity revealed distinct 2D flux-Vsw PDF's that were non-linear in nature and energy-dependent. Once a suitable delay time is used for the velocity the triangle distribution is no-longer evident, and flux probability depends upon velocity for all values of Vsw, with higher probabilities associated with higher fluxes. In addition, the flux-Vsw probability distribution function for lower energy electrons (31.7 keV) was quite similar to the flux and 2-day Vsw PDF for relativistic electrons, for fixed values of the solar wind density.

[40] 2. The enhanced solar wind density also resulted in a saturation of the most probable 31.7 keV electron flux at a lower value of Vsw than for low density conditions. The saturation of low energy electron fluxes corresponded to theoretical expectations associated with the Kennel-Petschek limit, and the increase in flux for a given Vsw was associated with enhanced transport of the solar wind density to the outer-radiation belt, due to internal magnetospheric acceleration mechanisms.

[41] 3. An increase in density for a given Vsw resulted in an increase in low energy fluxes (31.7 keV) and a decrease in higher energy fluxes (270 keV to 1.8–3.5 MeV). The decrease in flux with elevated density for relativistic particles was also evident when Vsw was delayed by 2 days, and suggests that ULF waves cause a reduction in relativistic electron fluxes on a statistical basis. The combination of these two results support a scenario in which fluxes are enhanced through a local acceleration of source and seed electrons, convected to the inner magnetosphere by elevated solar wind velocities, and redistributed through radial diffusion.

[42] **Acknowledgments.** The research was supported by UC-LANL Lab Research Fee. The authors would like to thank *Reeves et al.* [2011] for providing the LANL/GEO data set, and Richard Denton and Zhengui Qin for the OMNI2 solar wind data. The authors would also like to thank Andrei Runov and Drew Turner for useful discussions.

[43] Philippa Browning thanks the reviewers for their assistance in evaluating this paper.

References

Baker, D. N., R. D. Belian, P. R. Higbie, R. W. Klebesadel, and J. B. Blake (Eds.) (1986), *Hostile Energetic Particle Radiation Environments in Earth's Outer Magnetosphere*, 16 pp., Los Alamos Natl. Lab., Los Alamos, N. M.

Baker, D. N., J. B. Blake, L. B. Callis, J. R. Cummings, D. Hovestadt, S. Kanekal, B. Klecker, R. A. Mewaldt, and R. D. Zwickl (1994), Relativistic electron acceleration and decay time scales in the inner and outer radiation belts: SAMPEX, *Geophys. Res. Lett.*, *21*, 409–412.

Baker, D. N., J. H. Allen, S. G. Kanekal, and G. D. Reeves (1998a), Disturbed space environment may have been related to pager satellite failure, *Eos Trans. AGU*, *79*(40), 477, doi:10.1029/98EO00359.

Baker, D. N., X. Li, J. B. Blake, and S. Kanekal (1998b), Strong electron acceleration in the Earth's magnetosphere, *Adv. Space Res.*, *21*, 609–613.

Balikhin, M. A., R. J. Boynton, S. N. Walker, J. E. Borovsky, S. A. Billings, and H. L. Wei (2011), Using the NARMAX approach to model the evolution of energetic electrons fluxes at geostationary orbit, *Geophys. Res. Lett.*, *38*, L18105, doi:10.1029/2011GL048980.

Blake, J. B., D. N. Baker, N. Turner, K. W. Ogilvie, and R. P. Lepping (1997), Correlation of changes in the outer-zone relativistic-electron population with upstream solar wind and magnetic field measurements, *Geophys. Res. Lett.*, *24*, 927–930.

Borovsky, J. E., and M. H. Denton (2006), Differences between CME-driven storms and CIR-driven storms, *J. Geophys. Res.*, *111*, A07S08, doi:10.1029/2005JA011447.

Borovsky, J. E., M. F. Thomsen, and R. C. Elphic (1998), The driving of the plasma sheet by the solar wind, *J. Geophys. Res.*, *103*, 17,617–17,639, doi:10.1029/97JA02986.

Chen, L., R. M. Thorne, and J. Bortnik (2011), The controlling effect of ion temperature on EMIC wave excitation and scattering, *Geophys. Res. Lett.*, *38*, L16109, doi:10.1029/2011GL048653.

Claudepierre, S. G., M. K. Hudson, W. Lotko, J. G. Lyon, and R. E. Denton (2010), Solar wind driving of magnetospheric ULF waves: Field line resonances driven by dynamic pressure fluctuations, *J. Geophys. Res.*, *115*, A11202, doi:10.1029/2010JA015399.

Fälthammar, C.-G. (1965), Effects of time-dependent electric fields on geomagnetically trapped radiation, *J. Geophys. Res.*, *70*, 2503–2516.

Friedel, R. H. W., G. D. Reeves, and T. Obara (2002), Relativistic electron dynamics in the inner magnetosphere–A review, *J. Atmos. Sol. Terr. Phys.*, *64*, 265–282, doi:10.1016/S13646826(01)000888.

Fung, S. F., and L. C. Tan (1998), Time correlation of low-altitude relativistic trapped electron fluxes with solar wind speeds, *Geophys. Res. Lett.*, *25*, 2361–2364.

Green, J., and M. G. Kivelson (2004), Relativistic electrons in the outer radiation belt: Differentiating between acceleration mechanisms, *J. Geophys. Res.*, *109*, A03213, doi:10.1029/2003JA010153.

Horne, R. B., S. A. Glauert, and R. M. Thorne (2003), Resonant diffusion of radiation belt electrons by whistler-mode chorus, *Geophys. Res. Lett.*, *30*(9), 1493, doi:10.1029/2003GL016963.

Horne, R. B., R. M. Thorne, S. A. Glauert, N. P. Meredith, D. Pokhotelov, and O. Santolík (2007), Electron acceleration in the Van Allen radiation belts by fast magnetosonic waves, *Geophys. Res. Lett.*, *34*, L17107, doi:10.1029/2007GL030267.

Jordanova, V. K., and Y. Miyoshi (2005), Relativistic model of ring current and radiation belt ions and electrons: Initial results, *Geophys. Res. Lett.*, *32*, L14104, doi:10.1029/2005GL023020.

Kataoka, R., and Y. Miyoshi (2008), Magnetosphere inflation during the recovery phase of geomagnetic storms as an excellent magnetic confinement of killer electrons, *Geophys. Res. Lett.*, *35*, L06S09, doi:10.1029/2007GL031842.

Kellogg, P. J. (1959), Van Allen radiation of solar origin, *Nature*, *183*, 1295–1297.

Kepko, L., and H. E. Spence (2003), Observations of discrete, global magnetospheric oscillations directly driven by solar wind density variations, *J. Geophys. Res.*, *108*(A6), 1257, doi:10.1029/2002JA009676.

Kepko, L., H. E. Spence, and H. J. Singer (2002), ULF waves in the solar wind as direct drivers of magnetospheric pulsations, *Geophys. Res. Lett.*, *29*(8), 1197, doi:10.1029/2001GL014405.

Korotova, G. I., and D. G. Sibeck (1995), A case study of transient event motion in the magnetosphere and in the ionosphere, *J. Geophys. Res.*, *100*, 35–46.

Li, X., M. Temerin, D. N. Baker, G. D. Reeves, and D. Larson (2001), Quantitative prediction of radiation belt electrons at geostationary orbit based on solar wind measurements, *Geophys. Res. Lett.*, *28*, 1887–1890.

Li, X., D. N. Baker, M. Temerin, G. Reeves, R. Friedel, and C. Shen (2005), Energetic electrons, 50 keV to 6 MeV, at geosynchronous orbit: Their responses to solar wind variations, *Space Weather*, *30*, S04001, doi:10.1029/2004SW000105.

Liu, S., M. W. Chen, L. R. Lyons, H. Korth, J. M. Albert, J. L. Roeder, P. C. Anderson, and M. F. Thomsen (2003), Contribution of convective transport to stormtime ring current electron injection, *J. Geophys. Res.*, *108*(A10), 1372, doi:10.1029/2003JA010004.

Lyatsky, W., and G. V. Khazanov (2008a), Effect of geomagnetic disturbances and solar wind density on relativistic electrons at geostationary orbit, *J. Geophys. Res.*, *113*, A08224, doi:10.1029/2008JA013048.

Lyatsky, W., and G. V. Khazanov (2008b), Effect of solar wind density on relativistic electrons at geosynchronous orbit, *Geophys. Res. Lett.*, *35*, L03109, doi:10.1029/2007GL032524.

Mathie, R. A., and I. R. Mann (2001), On the solar wind control of Pc5 ULF pulsation power at mid-latitudes: Implications for MeV electron acceleration in the outer radiation belt, *J. Geophys. Res.*, *106*, 29,783–29,796.

Mauk, B., and N. Fox (2010), Electron radiation belts of the solar system, *J. Geophys. Res.*, *115*, A12220, doi:10.1029/2010JA015660.

Meredith, N. P., R. B. Horne, and R. R. Anderson (2001), Substorm dependence of chorus amplitudes: Implications for the acceleration of electrons to relativistic energies, *J. Geophys. Res.*, *106*, 13,165–13,178.

Meredith, N. P., M. Cain, R. B. Horne, R. M. Thorne, D. Summers, and R. R. Anderson (2003), Evidence for chorus-driven electron acceleration to relativistic energies from a survey of geomagnetically disturbed periods, *J. Geophys. Res.*, *108*(A6), 1248, doi:10.1029/2002JA009764.

Miyoshi, Y. S., V. K. Jordanova, A. Morioka, M. F. Thomsen, G. D. Reeves, D. S. Evans, and J. C. Green (2006), Observations and modeling of energetic electron dynamics during the October 2001 storm, *J. Geophys. Res.*, *111*, A11S02, doi:10.1029/2005JA011351.

Obara, T., T. Nagatsuma, M. den, E. Sagawa, and T. Onsager (2000), Effects of the IMF and substorms on the rapid enhancement of relativistic electrons in the outer radiation belt during storm recovery phase, *Adv. Space Res.*, *26*, 89–92.

Omura, Y., N. Furuya, and D. Summers (2007), Relativistic turning acceleration of resonant electrons by coherent whistler mode waves in a dipole magnetic field, *J. Geophys. Res.*, *112*, A06236, doi:10.1029/2006JA012243.

Paulikas, G. A., and J. B. Blake (1979), Effects of the solar wind on magnetospheric dynamics: Energetic electrons at the synchronous orbit, in *Quantitative Modeling of Magnetospheric Processes*, *Geophys. Monogr. Ser.*, vol. 21, edited by W. P. Olson, pp. 180–202, AGU, Washington, D. C., doi:10.1029/GM021p0180.

Qin, Z., R. E. Denton, N. A. Tsyganenko, and S. Wolf (2007), Solar wind parameters for magnetospheric magnetic field modeling, *Space Weather*, *51*, S11003, doi:10.1029/2006SW000296.

Reeves, G. D., et al. (1998), The global response of relativistic radiation belt electrons to the January 1997 magnetic cloud, *Geophys. Res. Lett.*, *25*, 3265–3268, doi:10.1029/98GL02509.

Reeves, G. D., S. K. Morley, R. H. W. Friedel, M. G. Henderson, T. E. Cayton, G. Cunningham, J. B. Blake, R. A. Christensen, and D. Thomsen (2011), On the relationship between relativistic electron flux and solar wind velocity: Paulikas and Blake revisited, *J. Geophys. Res.*, *116*, A02213, doi:10.1029/2010JA015735.

Shprits, Y. Y., R. M. Thorne, R. Friedel, G. D. Reeves, J. Fennell, D. N. Baker, and S. G. Kanekal (2006), Outward radial diffusion driven by losses at magnetopause, *J. Geophys. Res.*, *111*, A11214, doi:10.1029/2006JA011657.

Shprits, Y. Y., D. A. Subbotin, N. P. Meredith, and S. R. Elkington (2008), Review of modeling of losses and sources of relativistic electrons in the outer radiation belt II: Local acceleration and loss, *J. Atmos. Sol. Terr. Phys.*, *70*, 1694–1713, doi:10.1016/j.jastp.2008.06.014.

Shprits, Y. Y., D. Subbotin, and B. Ni (2009), Evolution of electron fluxes in the outer radiation belt computed with the VERB code, *J. Geophys. Res.*, *114*, A11209, doi:10.1029/2008JA013784.

Summers, D., R. M. Thorne, and F. Xiao (1998), Relativistic theory of wave-particle resonant diffusion with application to electron acceleration in the magnetosphere, *J. Geophys. Res.*, *103*, 20,487–20,500.

Takahashi, K., and A. Y. Ukhorskiy (2008), Timing analysis of the relationship between solar wind parameters and geosynchronous Pc5 amplitude, *J. Geophys. Res.*, *113*, A12204, doi:10.1029/2008JA013327.

Tan, L. C., X. Shao, A. S. Sharma, and S. F. Fung (2010), Relativistic electron acceleration by compressional-mode ULF waves: Evidence from correlated Cluster, Los Alamos National Laboratory spacecraft, and ground-based magnetometer measurements, *J. Geophys. Res.*, *116*, A07226, doi:10.1029/2010JA016226.

Thorne, R. M. (2010), Radiation belt dynamics: The importance of wave-particle interactions, *Geophys. Res. Lett.*, *37*, L22107, doi:10.1029/2010GL044990.

Thorne, R. M., Y. Y. Shprits, N. P. Meredith, R. B. Horne, W. Li, and L. R. Lyons (2007), Refilling of the slot region between the inner and outer electron radiation belts during geomagnetic storms, *J. Geophys. Res.*, *112*, A06203, doi:10.1029/2006JA012176.

Tsurutani, B. T., and E. J. Smith (1977), Two types of magnetospheric ELF chorus and their substorm dependences, *J. Geophys. Res.*, *82*, 5112–5128.

Ukhorskiy, A. Y., Y. Shprits, B. J. Anderson, K. Takahashi, and R. M. Thorne (2010), Rapid scattering of radiation belt electrons by storm-time EMIC waves, *Geophys. Res. Lett.*, *37*, L09101, doi:10.1029/2010GL042906.

Usanova, M. E., I. R. Mann, I. J. Rae, Z. C. Kale, V. Angelopoulos, J. W. Bonnell, K.-H. Glassmeier, H. U. Auster, and H. J. Singer (2008), Multipoint observations of magnetospheric compression-related EMIC Pc1 waves by THEMIS and CARISMA, *Geophys. Res. Lett.*, *35*, L17S25, doi:10.1029/2008GL034458.

Wright, A. N., K. J. Mills, M. S. Ruderman, and L. Brevdo (2000), The absolute and convective instability of the magnetospheric flanks, *J. Geophys. Res.*, *105*, 385–394.